POLITECNICO DI TORINO
Repository ISTITUZIONALE

Design of synchronous reluctance motors with multiobjective optimization algorithms

(Article begins on next page)

01 September 2024

Design of Synchronous Reluctance Motors with Multi-Objective Optimization Algorithms

Francesco Cupertino
Politecnico di Bari - DEI
Bari, Italy
cupertino@poliba.it

Gianmario Pellegrino
Politecnico di Torino - DENERG
Torino, Italy
gianmario.pellegrino@polito.it

Chris Gerada
University of Nottingham
Nottingham, UK
chris.gerada@nottingham.ac.uk

Abstract—**The automatic design of Synchronous Reluctance (SyR) machines is considered in this paper by means of Finite Element Analysis and Multi-Objective Optimization Algorithms (MOOA). The research focuses on the design of the rotor geometry which is the key aspect of the SyR machine design. In particular, the performance of three popular MOOAs is analyzed and compared in terms of quality of the final design and computational time. A procedure to minimize the computational burden of the optimized design process is introduced and applied to a three layer and to a five layer rotors. Two prototypes demonstrate experimentally the feasibility of the design procedure.**

Index Terms – **Synchronous Reluctance Motor, Motor Design, Automatic Design, Optimization Algorithms, Multi-Objective Optimization.**

I. INTRODUCTION

Synchronous Reluctance (SyR) motors are a viable alternative to inverter driven Induction Motors (IM) because they allow a size reduction and/or an improvement in efficiency [1,2]. While the stator is like that of a standard IM, the rotor geometry is non-conventional and characterized by multiple flux barriers. Many configurations are possible, in terms of the number of barriers, their shape and dimensions. The literature on SyR motor design is vast and includes different design methodologies [3-4]. Optimization Algorithms (OA) and FEA were used twenty years ago [5] but then rarely again due to the fact that the numerous degrees of freedom make the optimization problem big, requiring thousands of individual evaluations prior to convergence. With such a large scale of evaluations, FEA can be time consuming. More commonly, FEA and OAs have been associated for single and double layer rotor structures with Permanent Magnets [6] as they can be handled with a lower number of geometric variables.

Nevertheless, FEA is mandatory in the design of SyR machines, as confirmed by all authors in the literature, including the ones that base the design on analytical models [7-8]. Linear magnetic models are too inaccurate due to steel saturation. In addition to the progressive saturation of the magnetic core with load, local saturation (e.g. in the structural bridges) also occurs from very light loads and impacts motor performances.

For an effective optimization using jointly FEA and MOOA it is critical to: 1) simplify as much as possible the description of the rotor geometry; 2) minimize the FEA evaluation time of the candidate solutions; 3) choose the MOOA and its settings properly, for a tradeoff between time and accuracy.

In this respect, we have presented in [9-10] the Multi-Objective Genetic Optimization of multi-barrier rotors based on FEA aiming at defining a comprehensive approach to SyR rotor design within a reasonable computation time. The fast FEA evaluation of the candidate machines [9] and the two-step application of the Multi-Objective Optimization Algorithm (MOOA) [10] were the focus of these preliminary works. The goals of this paper are:

- To compare three different MOOAs and evaluate the impact of their settings on the efficiency of the optimization.
- To formalize a procedure for the fast and reliable convergence of the OAs.
- To evaluate how convergence time is affected by the number of rotor layers.

The optimization algorithms under investigation are Genetic Algorithm (GA), Differential Evolution (DE) and Simulated Annealing (SA). They are applied here to the design of SyR motors of small size. The optimization goals are the maximization of the torque per Joule loss ratio and the minimization of the torque ripple. A procedure for the robust convergence of the optimization within a given number of function calls is formalized for the three OAs and general conclusions on the comparison are drawn. The design examples are for two SyR rotors having three layers and five layers respectively. The latter is useful to evaluate how the fast MOOA+FEA procedure is robust towards a significant increase in the number of input variables with respect to three-layer rotors. The two machine examples were prototyped and experimentally evaluated. Iron losses are computed using FEA, compared and commented upon. The 3-layer rotor produced by the OAs is similar to some existing designs in the literature, whereas the 5-layer one has a non-conventional barrier distribution from which interesting insights can be drawn.

II. PROBLEM STATEMENT

The two objectives of the optimization are the torque per Joule loss ratio and the torque ripple. The stator geometry is defined and originates from a PM-assisted machine for compressor application that was available in our labs. The

ratings of the original PM-assisted machine are 2.5 Nm at 5400 rpm and liquid cooled with an inlet temperature 90°C. The target ratings of the SyR motor designed here and reported in Table II are 4 Nm at 5000 rpm with forced ventilation. The continuous peak current i_0 is 16.8 A and corresponds to the rated Joule losses. The rated dc-link voltage is 270 V. The windings are distributed, not chorded and with two slots per pole per phase. The airgap thickness is 0.5 mm. The design is optimized with reference to a current value that is two or three times i_0, corresponding to transient overload conditions. It has been demonstrated in [11] that optimizing for overload conditions produces machine designs whose torque ripple is more insensitive to load variations.

Other potential objectives to be optimized for could have been efficiency, the cost of the materials or the weight of the active parts [12-13]. The latter two objectives would need to reconsider the stator geometry and the stator to rotor split ratio. This is out of scope for the exercise presented in this paper, however the conclusions drawn from the research presented in this paper can be translated to any optimization problem. When dealing with the efficiency it is important to point out that the torque maximization at given current and stator geometry inherently maximizes the torque per Joule loss ratio. This will have a major impact on efficiency. However, if a comprehensive optimization of efficiency is to be done one would require the evaluation of core losses at each function call of the MOOAs. Such objective is critical for PM-assisted SyR machines and multi-layer IPM machines especially if operated within their extended flux weakening speed range. [14-16]. However, this is less critical for SyR machines and particularly for the considered speed range in this paper. As previously mentioned the maximum torque per copper conducting loss has already a major impact on efficiency and torque ripple cannot be dismissed as high ripple readily occur when this is not taken into account. This is not an acceptable compromise.

One final remark is about the maximization of the power factor which is of importance for SyR machines. This is inherently around its best after the maximization of the average torque for a given current, that corresponds to the maximization of the dq inductance difference, not far from the saliency (and power factor) maximization condition, given the constrained stator geometry [17].

A. Parametrization of the rotor geometry

The rotor geometry is defined in Fig. 1 for an example motor with two pole-pairs and 5 layers. The set of parameters used to describe the rotor geometry has a critical role in the design optimization. The barrier shape types in the literature are various and full of parameters and a strong simplification is needed here to keep the optimization process as simple as possible. Each variable should have a reasonable impact on at least one of the performance indexes of the optimization. It was demonstrated in [10] that circular barriers, with two input variables per layer can get close to the performance of more complex geometries despite their very basic set of parameters. For circular layers the geometric inputs are:

- the layer angular positions at the airgap $\Delta\alpha_j$;
- the layer heights hc_j;

Last but not least, the phase angle γ of the current vector with respect to the synchronous d axis (maximum permanence axis), is also included in the optimization variables. Each motor is evaluated using a single current angle. At the end of the optimization γ was always very close to the Maximum Torque per Ampere (MTPA) angle condition γ_{MTPA}, which is the one maximizing the torque per Joule loss.

The number of variables to be optimized is then $2\,n_{lay} + 1$, n_{lay} being the number of rotor layers. This means a 7-dimensional and an 11-dimensional space of inputs for the 3- and 5-layer machines respectively.

The set of search bounds used in the paper is reported in Table I. Wherever p.u. is indicated, it means that the value is in per-unit of the aggregate height or angle available for all the layers. The first angular input $\Delta\alpha_1$ is in degrees and determines the angular space left to the other angular inputs: the other p.u. angles $\Delta\alpha_j$ ($j = 2$ to n_{lay}) define the layer tips distribution over the remaining part of the half pole angular pitch. Once the barrier ends positions $\Delta\alpha_j$ are set, the p.u. thicknesses hc_i are interpreted as follows: if they are all 1 p.u. then the air barriers are all the same thickness and occupy as much radial space as they can. A minimum thickness of the flux guides is fixed, 1 mm for the examples here. The 1 mm clearance condition avoids overlapping barriers and non-feasible rotors, manufacturing-wise, that could come from incompatible combinations of the inputs. If all the p.u. heights are of a different value, say the minimum (0.2), then the barriers are again all the same thickness and of a value which is of 20% of the previous example. All other situations are combination of the previous ones.

TABLE I - LIMITS OF THE SEARCH SPACE FOR THE GLOBAL SEARCH (GS)

Parameter	Min value	Max value	Units
$hc_i\,(i=1,..,n_{lay})$	0.2	1	p.u.
$\Delta\alpha_1$	15	27	degrees
$\Delta\alpha_j\,(j=2,..,n_{lay})$	0.33	0.67	p.u.
γ	20	80	degrees

B. Fast FEA Evaluation of the Candidate Machines

The performance indexes to be optimized, torque and torque ripple, are evaluated in a single current condition (amplitude and phase angle γ in synchronous coordinates) so as to minimize computation. The current amplitude selected in the examples is twice the machine rated current ($2\,i_0$), as a trade-off between continuous torque and maximum overload conditions ($3\,i_0$). This also guarantees a low torque ripple at lower load levels [11].

C. Two-Objective Cost Function Evaluation

The torque of each candidate solution is calculated using FEA in n equally spaced rotor positions, covering one stator slot pitch (τ_{st}). The average value and the standard deviation of such n-points waveforms are the two cost functions of the optimization. The stator slot pitch was chosen because it is

representative of the most significant harmonic component of the torque ripple. The choice of *n* is discussed in [9]. Despite the very few positions considered (e.g. five positions are used in this paper), the aliasing of significant torque harmonics is avoided via a random position offset at each evaluation [9].

TABLE II – SyR MACHINES PROTOTYPES RATINGS

Continuous torque	4.5	Nm
Rated speed	5000	rpm
Rated voltage	270	V (dc-link)
Continuous current	16.8	A (pk)
Stack outer diameter	101	mm
Rotor diameter	58.6	mm
Airgap	0.5	mm
Stack length	65	mm
Stator Slots	24	
Steel grade	M470-50	(Stator)
	M270-35	(Rotor)

In turn, the MOOAs evaluate the candidate solutions via the FEA calculation of the electromagnetic torque for a single current amplitude and phase condition over five rotor positions with the first position decided randomly. All the final Pareto fronts evaluated so far showed that:

1) The γ_{MTPA} angle is correctly estimated by the MOOA.
2) The torque ripple of all output machines is minimized.
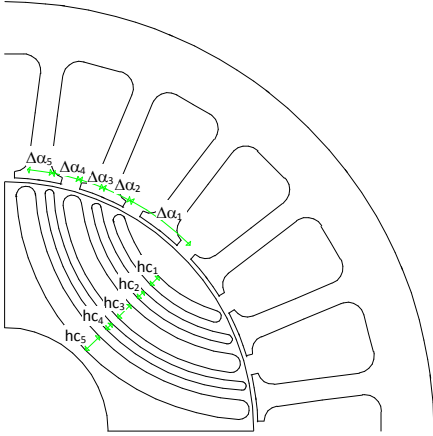3) Interestingly, the torque ripple is minimum along the MTPA trajectory at all values of the current amplitude.

Figure 1. Rotor geometry with 5 layers: the $\Delta\alpha_j$ angles define the layer angular positions, hci are the layer heights.

D. Optimization procedure and MOOA settings

The proposed MOOA-based design procedure consists of a first stage called Global Search (GS) and a successive Local Search refinement stage (LS). During the GS, the bounds of the search space are coarse, meaning that all the feasible rotors are considered as potential solutions. Table I reports the bounds values used for the GS optimization. The GS is repeated several times to avoid local minima, as explained in Section III.

After the GS stage one of the GS-optimized machines is selected for further refinement. The LS stage is an additional MOOA run, with the input bounds restricted around the set of the GS-selected machine inputs. The GS + LS procedure is quicker and more reliable than a single long run of the MOOA.

III. META-HEURISTIC ALGORITHMS

Meta-heuristic optimization algorithms use a set of N_p candidate solutions (*population*) that are iteratively modified according to probabilistic rules aiming at finding the global minimum of the chosen objective function. There exists no best algorithm that is valid for any class of problems (no free-lunch theorem [18]). In addition no algorithm can avoid the risk of falling into sub-optimal solutions (local minima). Genetic algorithms [19] simulated annealing [20] and differential evolution [21] represent three popular class of algorithms that have been considered and compared in this paper to find the best trade-off between computational cost and reliability of the final results. They can be easily implemented thanks to the wide open-source references available in the literature [22].

All the mentioned algorithms can solve multi-objective problems by introducing the concept of *dominance*. A solution is *non-dominated* when there is no other solution having better values for all the cost functions or objectives. We adopted the approach proposed in the NSGA-II algorithm for non-dominated and crowing distance sorting [23].

A. Genetic Algorithms Settings

In genetic algorithms (GAs) the populations evolve using the biology-inspired operators of crossover and mutation. We adopted the GA implemented in the Matlab optimization toolbox using the intermediate crossover and adaptive feasible mutation which are the default operators. The parameter that guides the crossover is the crossover fraction. This specifies the fraction of each population that will be generated using the crossover operator. The value used in the tests was 0.8.

B. Differential Evolution Settings

According to the original definition of DE [21], each individual x_k of the N_p-members population evolves according to the combination of other three individuals out of the N_p, x_r, x_s, and x_t, randomly extracted from the population. The provisional offspring x'_{off} is generated by *mutation* as:

$$x'_{off} = x_t + F(x_r - x_s) \qquad (1)$$

where the scalar factor F controls the length of the exploration vector $(x_r - x_s)$ and thus determines how far from the individual x_t the offspring can be generated. The gain F was randomly selected in the range [0 1.5] using the procedure introduced in [24]. Other values of F were tested,

as reported in subsection IV.F. Finally, the actual offspring x_{off} is generated according to the **crossover** procedure (2):

$$x_{off}[i] = \begin{cases} x'_{off}[i] \; if \; rand \leq C_r \\ \quad x_k[i] \; otherwise \end{cases} \quad (2)$$

where *rand* is a random number between 0 and 1; *i* is the index of the gene under examination; C_r is the crossover rate selected equal to 0.95.

C. Simulated Annealing Settings

SA is inspired by annealing in metallurgy and is based on the random perturbation of each individual in the population according to the following rule:

$$x_{off} = x_k + \sqrt{T_j} \; rand(N_p) \quad (3)$$

Where $rand(N_p)$ is a vector of N_p random numbers, and T_j is the current "equivalent temperature". Starting from the initial temperature T_0, at each iteration, this is decreased according to (4):

$$T_j = T_0(0.87)^j \quad (4)$$

IV. SIMULATION RESULTS

In this section the three MOOAs are applied to the optimization of a five layer SyR rotor, with the machines specifications reported in Table II. Three acronyms are introduced:

- MOGA: Multi-Objective Genetic Algorithm;
- MODE: Multi-Objective Differential Evolution;
- MOSA: Multi-Objective Simulated Annealing.

The search space described in Table I is used for all the algorithms. A predetermined number of function calls equal for all is used as stopping criterion. In this way the computational cost is nearly the same for the three and the performance comparison is based only on the quality of the final results.

A. Description of the Simulation Set-Up

As mentioned beforehand, each function call consists of five FEA simulations for five rotor positions. Static-magnetic simulations were used [25]. One candidate takes 2.6 seconds on a Intel Xeon E5-1620 workstation (4 cores, 3.60 GHz, 16 GB ram), thanks to the 5-core parallel calculation (the fifth core is emulated by the Xeon processor).

All the algorithms were tested in different conditions and only the most representative results are shown here for sake of brevity. Reference is made to a population size $N_p = 60$ and to the search bounds reported in Table I, defined as the Global Search bounds.

The results reported in Figs. 2 and 3 refer to the MOOAs stopped after 1200 function calls (i.e. 1200 machines evaluated, Fig. 2) and after 3000 calls (Fig. 3). The shorter runs (1200 calls) require about **one hour** each, while the longer ones (3000 runs) **less than 2.5 hours** on the selected processor. To obtain Pareto fronts with a good density of solutions a penalty function was applied despite the small population size. The penalty function was applied to solutions with a torque ripple over 6% or an average torque under 4 Nm as they are way out of specification. In this way the final Pareto front is concentrated in the area of interest of the torque-torque ripple space.

B. Effect of noise in cost function evaluation

It is worth to point out that the cost function is noisy due to the random choice of the rotor position offset. On the one hand the random offset shortens the evaluation time, as already mentioned. On the other hand, however, it implies that the machine performance can be accidentally under- or over-estimated. If a strong over-estimate occurs, a non-optimal machine can remain on the Pareto front for long enough to be on the final front of solutions illegitimately. According to NSGA-II, some of the better solutions from the current iteration are kept unaltered to the next iteration [23]. This strategy is known as elitist selection.

Therefore at the end of each optimization run, the Pareto-optimal machines were re-evaluated accurately over 15 time-stepped rotor positions instead of the 5 used in the optimization stage to filter-off any over-estimated solutions. After re-evaluation, the dominated solutions were disregarded and they are not represented in Figs. 2 and 3, or in all the other reported results.

C. Analysis of the Simulation Results

The 1200- and 3000-evaluation results of Figs. 2 and 3 report *ten GS runs for each MOOA*. The figures aggregate all the obtained Pareto fronts in the torque - torque ripple domain. Negative torque values are used as optimization algorithms minimize the cost function values. Figures 2 and 3 give a quick comparative summary of the performance of the different algorithms. The best algorithm will be the one giving the best machines but also the one giving repeatable results for all its GS Pareto fronts. This kind of consistency is particularly needed here, because it allows for the reduction of the number of GS runs needed to trust the GS stage and proceed to the LS refinement.

A comparison of figures 2 and 3 reveals that, intuitively, the Pareto fronts are more concentrated when the number of function calls is increased, for all the OAs. The MODE gives the best results both in terms of torque/torque ripple values and repeatability, as its Pareto fronts are already stable after just 1200 evaluations. The MOSA has a great improvement when passing from 1200 to 3000 evaluations. The MOGA has more sparse fronts and does not improve significantly going from 1200 to 3000 evaluations. It is worth mentioning that results obtained with over 3000 calls gave no further improvement. This may be due to the reduced ability of the selected algorithms to face the problems due to the noisy cost function. Although the approach proposed here gives satisfactory results, it is planned to modify the algorithms in the direction of non-persistent elitist selection for future work.

D. Comparison over Ten GS Runs

Summing up the results of Figs. 2 and 3, the MODE gives the best results, and its Pareto fronts are already

stabilized after 1200 evaluations. As a reference for comparison of the three MOOAs the benchmark performance is set to 7.8 Nm and 4.0% ripple. Table III rates each algorithm according to the percentage of GS runs
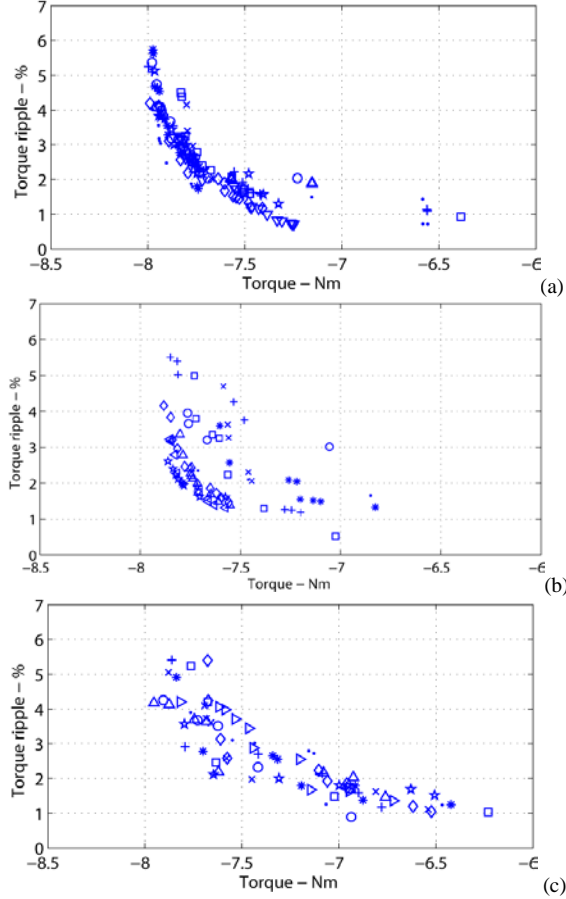
having at least one solution which is over the benchmark. For the MODE, 9 runs out of 10 are within the benchmark mask at 1200 function calls, and 10 out of 10 after 3000 calls. All the other MOOAs have a weaker performance.

Figure 2.   Summary of the Pareto fronts of ten optimization runs, obtained using (a) MODE, (b) MOGA, (c) MOSA. The runs were stopped at 1200 function calls. The markers indicate the different runs.
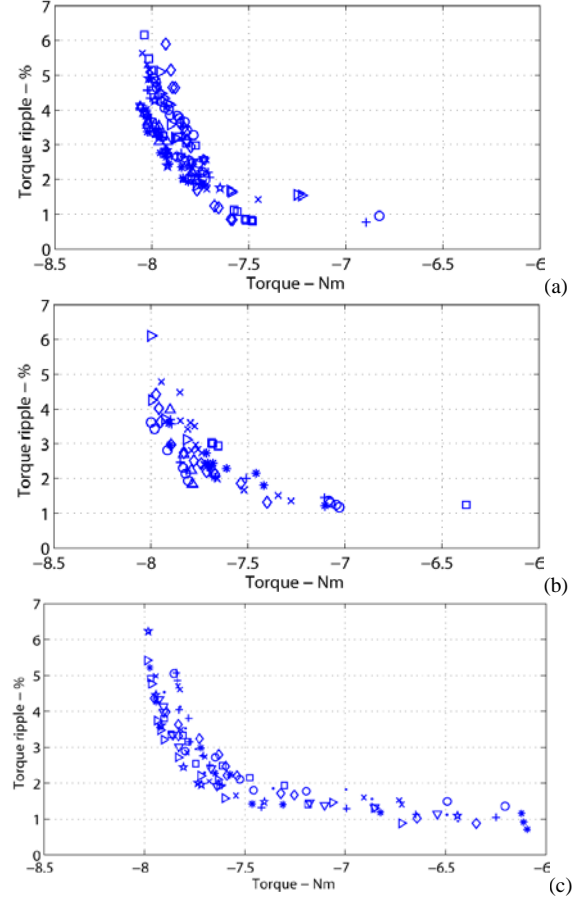

Figure 3.   Summary of the Pareto fronts of ten optimization runs, obtained using (a) MODE, (b) MOGA, (c) MOSA. The runs were stopped at 3000 function calls. The markers indicate the different runs..

TABLE III - PERCENTAGE OF SATISFACTORY GS RUNS
(TORQUE>7.8, TORQUE RIPPLE<4%)

Algorithm	1200 function calls	3000 function calls
MODE	90%	100%
MOGA	40%	80%
MOSA	20%	100%

E. Local Search refinement

From the results of the GS sessions, a single Local Search run is performed. Considering that the MODE produces 9 satisfactory GS runs out of 10 when stopped at 1200 calls, the design procedure proposed here uses four of the MODE 1200-GS runs to determine the GS-selected machine to start the LS refinement.

Given four Pareto fronts of the GS type, the GS-selected machine is selected according to the ripple specification of the application. For example, in Fig. 4 the GS-solution was chosen after a ≤4% ripple specification. If such a specification was more stringent, the GS solution would have been traded with one with less torque ripple but also

with less torque. The search bounds of the LS run are ±15% of the GS-selected machine inputs. Figure 4 shows the Pareto front of the LS run compared with the four MODE-GS fronts from which the GS-selected machine has been picked up. Both GS and LS fronts have been re-evaluated over 15 rotor positions, as previously mentioned. From this final LS-Pareto front one machine was selected (hereinafter the LS-machine) which improves the average torque by 1% and the torque ripple by 35% with respect to GS-selected machine. It is important to put in evidence that none of the GS runs had any solution better than the final LS-machine. Returning to GS stage, the four repetitions of the GS runs ensure that the unlucky run out of ten of Fig. 2a and Table III is statistically avoided, and that the LS refinement has a starting base that is as good as possible: better than with a single GS run but not worse than with 10 GS runs or more. The whole computation of 4 GS runs and one LS run, requires about 5 hours to be completed. When a very low ripple is not specifically required by the application, the

LS-stage can be avoided with no practical penalty in terms of average torque.

F. Sensitivity to the MOOA settings.

The optimization tests revealed a generally good robustness of the results towards the calibration of the algorithms. This section reports the analysis of the sensitivity of the results to the calibration of the MODE parameters. Similar tests are not reported for the other algorithms, for the sake of brevity.
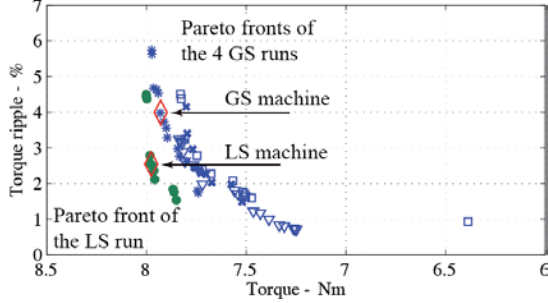

Figure 4.   Selected GS run and LS run Pareto fronts obtained using MODE and 1200 function calls. GS- and LS-machines are evidenced with red diamonds.
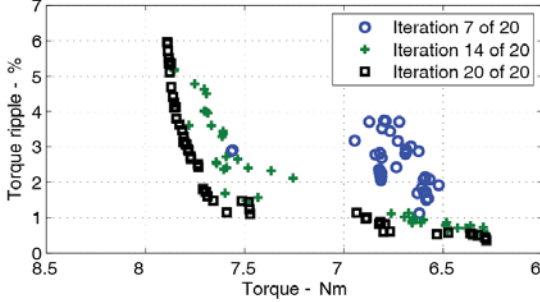

Figure 5.   Evolution of the N_p=60 popolation of a 1200-call MODE run.

TABLE III - PERCENTAGE OF SATISFACTORY MODE RUNS (>7.8 NM, RIPPLE <4%) USING DIFFERENT CONFIGURATION PARAMETERS.

Settings	
$F \in [0\ 1.5], C_r = 0.99$	100%
$F \in [0\ 1.5], C_r = 0.95$	90% (*)
$F \in [0\ 1.5], C_r = 0.90$	90%
$F \in [0\ 1.5], C_r = 0.80$	80%
$F \in [0\ 1.5], C_r = 0.50$	70%
$F \in [0.1\ 0.9], C_r = 0.95$	100%
$F = 1.5, C_r = 0.95$	20%
$F = 1, C_r = 0.95$	70%
$F = 0.5, C_r = 0.95$	100%

(*) benchmark settings used in Figs. 2-5.

The evolution of the population over the iterations of a typical GS MODE run is shown in Fig. 5. The population size was $N_p = 60$ and 1200 function calls was the stopping criterion. The solutions tend to spread along the estimate of the Pareto front as the algorithm evolves. This process is almost completed after 20 iterations with these MODE settings.

The two key settings of the MODE are F and C_r, defined in subsection III.B. Table III reports the percentage of

satisfactory GS-1200 runs obtained when using different values of F and C_r. The increase of C_r is beneficial, but the performance remains acceptable in the whole considered range. Regarding F, the results in Figs. 2 to 5 refer to F randomly selected in the range [0 1.5]. The [0.1 0.9] range suggested in [24] actually improves the results, as evidenced in Table III. It is also possible to obtain comparable performances using a constant value of F, provided that this is small enough (0.5 is better than 1.0 and 1.5). This analysis shows the robustenss of the adopted design approach and evidences that a further improvement is possible, with a finer tuning of the MODE algorithm.

Another key aspect of calibration is the tradeoff between the population size and the number of function calls. Starting from the benchmark population size $N_p = 60$ used in Figs. 2 to 5, a smaller population would reduce the accuracy, whereas a larger one would increase the computational time. Fig. 6 shows that it is true that larger populations and larger call numbers tends to more accurate results: the reported ten MODE runs with $N_p = 200$ and 6000 function calls each include many solutions which are in the neighborhoods of the LS-machine of Fig. 4. This combination of parameters requires a computational time of 5 hours per run, comparable to a whole 4 times GS + LS procedure with $N_p = 60$. Yet a single long run is not statistically immune from local minima, as experienced by the authors after repeated MOOAs simulations. For example the front of red crosses "+" in Fig. 6 is worse than the aggregate four GS fronts of Fig. 4.
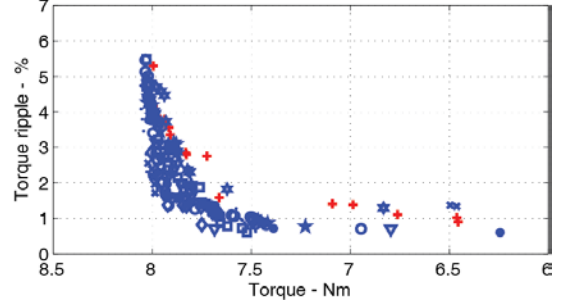

Figure 6.   Summary of the Pareto fronts of ten optimization runs, obtained using N_p=200 and 6000 calls. The markers indicate the different runs.
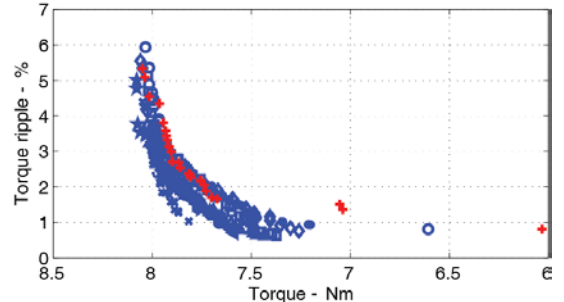

Figure 7.   Summary of the Pareto fronts of ten optimization runs, obtained using no random position offset for the rotor and 15 rotor positions instead of 5. Each run was stopped after 2000 function calls. The markers indicate the different runs.

All considered, four quick runs and one long run give similar results, but the former procedure is considered more

robust. Finally the impact of the cost function noise produced by the random position offset is investigated by launching several MODE runs with 15 FEA simulated rotor positions, instead of 5, and without the random position offset. The results are reported in Fig. 7. Each run was stopped after 2000 evaluations, so that the computational burden of one run is comparable to a whole 4 GS + LS procedure. Again, in this case, a single run is not always better than the LS-solution found with the 4 GS + LS procedure.

The aim of this work is to contribute to the formulation of a software tool for the support of motor designers from the industry. Then the quicker the response of the optimization procedure, the more helpful the automatic design tool will be. The MODE configuration parameters used in the previous sub-sections represent a reasonable compromise between fast and accurate results.

V. EXPERIMENTAL RESULTS

Two SyR rotor prototypes were built for validating the proposed design procedure. The one with 5 layers is the LS-machine of Fig.4. A three-layer rotor was also MODE designed and tested, with the same 4 GS+LS procedure. The two machines are indicated with 5C and 3C, respectively.
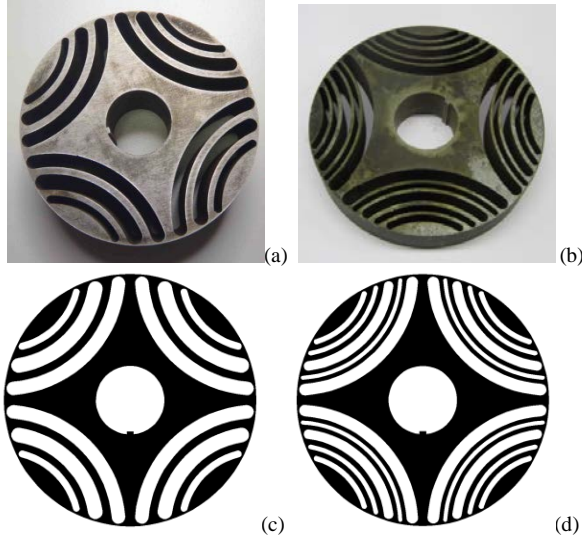
(a)   (b)

(c)   (d)

Figure 8. a) Rotor laminations of prototype 3C; b) Rotor laminations of prototype 5C; c) cross section of the 3C rotor; d) cross section of the 5C rotor.

A. Discussion of the Layers Geometries

Fig. 8 reports the pictures of the laminations ("a" and "b") and their cross-sections ("c" and "d"). The 3C rotor has a regular pitch, consistent with the literature for minimum ripple machines [2,4,26]. The rotor pitch in the area where this is regular would correspond to 32 equivalent slots, that is one of the good combinations suggested in [4] for a 24 slots stator. Dealing with the 5C rotor, the five layers thicknesses are neither progressive [4] or all equal [3]. The MODE has designed a machine with three main layers (1, 3, 5), and two very thin layers in between. This layer distribution has not been reported in the literature. One can argue that it seems that the MOOA tried to group the layers together to form a three-layer-like distribution. In fact, the ends of the three main layers (1, 3, 5) occupy again the positions of a 32 regular slots rotor. The thinner layers are exactly half way between the main ones. FEA shows that the presence of the two extra layers helps mitigating the torque ripple, as demonstrated by the fact that all the MOOAs converge very easily to low ripple solutions, despite of the numerous degrees of freedom. In turn, the more complicated problem (5C), defined by 10 geometric variables, converges in a time that is very similar to the one of the simpler problem (3C, 6 variables). The total computation time needed for running the 4GS+LS procedure is practically the same for both the 3C and the 5C rotors.

B. Measured versus Simulated Torque

The torque ripple maps versus the i_d, i_q current components were measured using a dedicated test bench, depicted in Fig. 9. The rotor speed is controlled at 10 rpm by a geared DC motor during the tests. The motor under test is current vector-controlled, using a dSPACE 1104 development board. The dq current set-points and the torque-meter logged along one motor revolution are managed automatically by means of a Matlab script. The 10 Nm rating of the torque-meter limits experiments not to exceed the i_d=20 A, i_q=30 A current area.
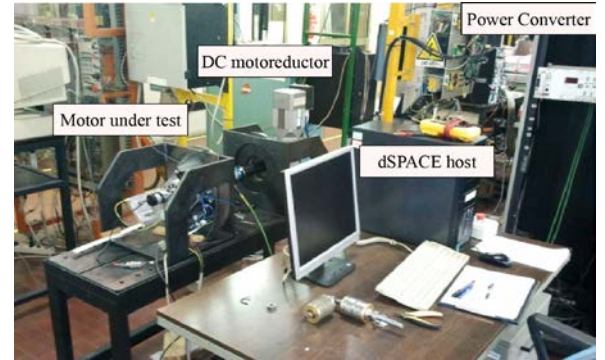
Figure 9. Test bench used to measure the torque ripple maps.

The measured torque and torque ripple values are reported in Figs. 10 to 14 for comparison with the FEA results.

The average torque from the experiments is slightly lower than the simulated one (Figs. 10 and 11). In addition the torque ripple is slightly worse than the simulated ones (Figs. 12 and 13). However, both FEA and experiments present a similar minimum-ripple trajectory in the i_d, i_q domain (Fig. 12 for the 3C rotor, Fig. 13 for the 5C rotor).

Figure 14 shows the measured and FEA torque waveforms compared at three current levels. This summarizes the conclusions of the former figures, i.e. there are some expected discrepancies between FEA and the measured results, however, the experiments confirm the expected machine performances consistently:

- The torque ripple increases with the current loading, however, this is well minimized, at least up to continuous current (16.8 A).
- Torque ripple is minimum along the MTPA, due to the specific optimization technique.
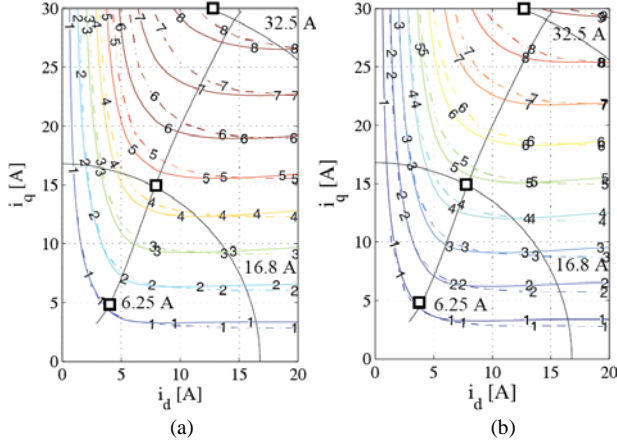- The 3C and 5C rotors have similar performance at all loads, both in FEA and in the experiments.

(a)

(b)

Figure 10. Torque contours evaluated with FEA (continuous line) and experiments (dashed lines). The MTPA line is in evidence. The three squares indicate the working points reported in Fig. 14. a) Prototype 3C; b) Prototype 5C.
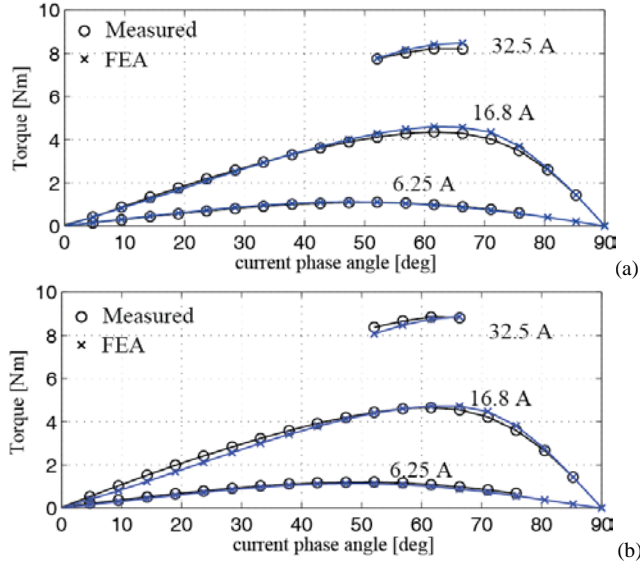
Figure 11. Torque as a function of the current phase angle, at two different values of current amplitude. a) Prototype 3C; b) Prototype 5C.

In terms of the discrepancy between measured and FEA results, these are mainly caused by the non-exact knowledge of the magnetization curve of the steel, by the effects of manufacturing tolerances as well as those due assembly tolerances. The steel magnetic properties in deep saturation are very important here in order to predict accurate performance. In addition it is also possible that local mechanical and thermal stress close to the bridges during manufacturing might alter the magnetic properties locally. The laminations were wire-cut using high precision Electric

Discharge Machining (EDM), nevertheless it is reasonable that the increased torque ripple and reduced torque are justified by such prototypes' non-idealities. From the tolerances standpoint, the actual thickness of the structural bridges, for example, is very critical for the ripple waveform.
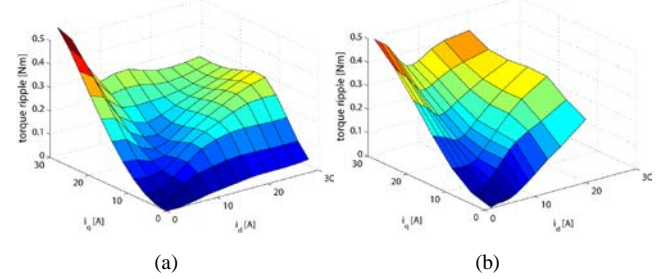
(a)

(b)

Figure 12. Prototype 3C: torque ripple surface over the i_d, i_q plane, according to FEA (a) and measurements (b).
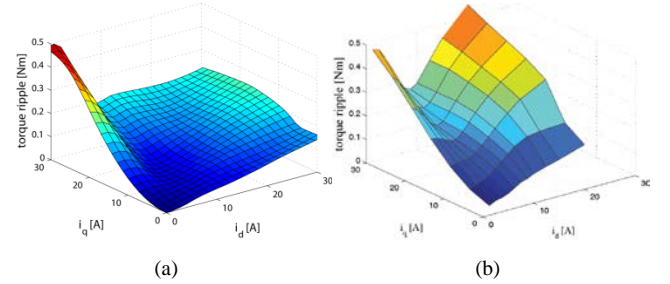
(a)

(b)

Figure 13. Prototype 5C: torque ripple surface over the i_d, i_q plane, according to FEA (a) and measurements (b).
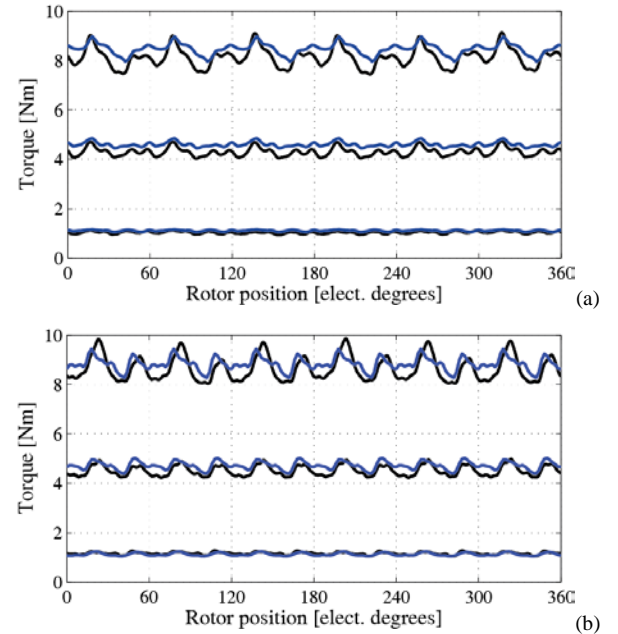
(a)

(b)

Figure 14. Torque waveforms for the i_d, i_q combinations indicated with black squares in Fig. 10. a) Prototype 3C; b) prototype 5C.

C. Core Loss and Efficiency

The efficiency maps of the two prototypes are reported in Fig. 15, in the torque versus speed plane. The MTPA control law is assumed for each torque level, and the stator Joule losses are evaluated accordingly. The 5C machine has a little advantage respect to the 3C competitor.

The core losses were FEA mapped over the whole (i_d, i_q) plane using Magnet, by Infolytica [27]. Magnet adopts a two-term modified Steinmetz model that fits the loss data published by the steel manufacturers, and the core loss are calculated on the stator and the rotor taking into account the actual field waveforms in each single finite element, all harmonics included. The core loss map over (i_d, i_q) was run at rated speed, and then generalized to any speed level according to the two-term loss model of Magnet, where the classical loss term is scaled according to the square of the frequency and then of the speed, and the modified hysteresis term is scaled according to the frequency raised to the α power (the exponent α is equal to 0.996 for the stator grade M470-50 and to 1.207 for the rotor grade M270-35, according to the library of materials of Magnet).
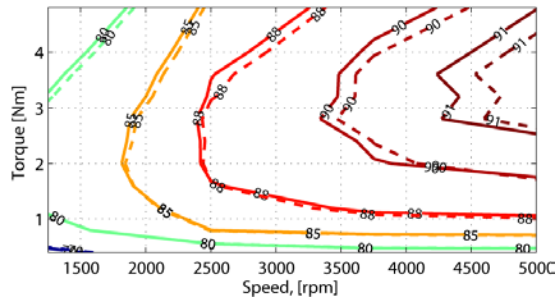

Figure 15. Efficiency map in the torque-speed plane for the prototyped (dotted lines) 3C and (solid lines) 5C machines.

The segregation of stator and rotor core loss and copper loss is reported in Fig. 16 at the rated speed of 5000 rpm, for continuous and partial load. The total core loss is under control, being lower than the Joule loss, for both machines. Core losses are mostly on the stator, and they are lower in the 5C machine, overall. This stands for lower harmonic losses. The rotor loss is quite negligible, but it is lower in the 3C machine. This is consistent with the literature: a rotor with a higher number of "rotor slots" has higher rotor harmonic losses [16].
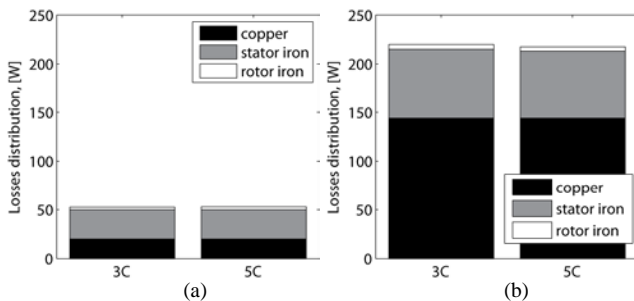

Figure 16. Losses distribution at 5000 rpm: a) 1 Nm; b) 4.5 Nm

All considered, the two prototypes have very similar performances, in terms of torque, torque ripple and efficiency. The better efficiency of the 5C machine in Fig. 15 could justify the adoption of this solution, while the simpler geometry of the 3C could encourage the opposite choice from a manufacturing perspective.

The 3-layer-like nonconventional distribution of the 5 layers in the 5C rotor confirms that this stator configuration (2 slots per pole per phase) is best matched with a 3-layer rotor with equally distributed barrier-ends, as also confirmed in the literature [4].

VI. CONCLUSION

The paper presented a procedure for the automatic design of multi-layer Synchronous Reluctance motors based on FEA and MOOAs of different nature. Three popular MOOAs selected from the literature have been compared, and Differential Evolution gives the best results in terms of convergence time and repeatability of the results. A comprehensive rotor design procedure has been formulated giving a robust optimization of the performance within short time. The proposed 4GS + LS procedure has been validated on two example rotors. Both machines had comparable performance within similar computation times. The experimental results show that the optimized machines have a minimum ripple region along the MTPA control trajectory and this is a consequence of the proposed MOOA + FEA approach. The MOOA and FEA approach produced a competitive five layer machine, using a non-standard distribution of the five layers widths and end-positions. However the three layer rotor is the best match for the specific number of stator slots considered in the paper.

REFERENCES

[1] Vagati, A.; Fratta, A.; Franceschini, G.; Rosso, P., "AC motors for high-performance drives: a design-based comparison," Industry Applications, IEEE Transactions on , vol.32, no.5, pp.1211,1219, Sep/Oct 1996

[2] Moghaddam, R.R.; Magnussen, F.; Sadarangani, C.; , "Theoretical and Experimental Reevaluation of Synchronous Reluctance Machine," Industrial Electronics, IEEE Transactions on , vol.57, no.1, pp.6-13, Jan. 2010

[3] T. A. Lipo, T. J. E. Miller, A. Vagati, I. Boldea, L. Malesani, and T. Fukao, "Synchronous reluctance drives" tutorial presented at IEEE IAS Annual Meeting, Denver, CO, Oct. 1994.

[4] Vagati, A.; Pastorelli, M.; Francheschini, G.; Petrache, S.C., "Design of low-torque-ripple synchronous reluctance motors," Industry Applications, IEEE Transactions on , vol.34, no.4, pp.758-765, Jul/Aug 1998.

[5] Kamper, M.J.; van der Merwe, F.S.; Williamson, S.,"Direct finite element design optimisation of the cageless reluctance synchronous machine", IEEE Transactions on Energy Conversion, Vol.   11, n. 3, September 1996.

[6] Vagati, A.; Canova, A.; Chiampi, M.; Pastorelli, M.; Repetto, M., "Design refinement of synchronous reluctance motors through finite-element analysis," Industry Applications, IEEE Transactions on , vol.36, no.4, pp.1094,1102, Jul/Aug 2000

[7] Lovelace, E.C.; Jahns, T.M.; Lang, J.H.; , "A saturating lumped-parameter model for an interior PM synchronous machine," Industry Applications, IEEE Transactions on , vol.38, no.3, pp.645-650, May/Jun 2002

[8] Sizov, G.Y.; Ionel, D.M.; Demerdash, N.A.O.; , "Multi-objective optimization of PM AC machines using computationally efficient - FEA and differential evolution," Electric Machines & Drives Conference (IEMDC), 2011 IEEE International , vol., no., pp.1528-1533, 15-18 May 2011

[9] Pellegrino, G.; Cupertino, F., "FEA-based multi-objective optimization of IPM motor design including rotor losses," IEEE Energy Conversion Congress and Exposition (ECCE), 2010, vol., no., pp.3659-3666, 12-16 Sept. 2010

[10] F. Cupertino, G.M. Pellegrino, E. Armando, C. Gerada, "A SyR and IPM machine design methodology assisted by optimization algorithms" IEEE Energy Conversion Congress and Exposition (ECCE), 2012, vol., no., pp.3686-3691, 15-21 Sept. 2012.

[11] Pellegrino, G.; Cupertino, F.; Gerada, C., "Barriers shapes and minimum set of rotor parameters in the automated design of Synchronous Reluctance machines," Electric Machines & Drives Conference (IEMDC), 2013 IEEE International , vol., no., pp.1204,1210, 12-15 May 2013.

[12] J. Legranger, G. Friedrich, S. Vivier, and J.C. Mipo, "Combination of Finite-Element and Analytical Models in the Optimal Multidomain Design of Machines: Application to an Interior Permanent-Magnet Starter Generator", IEEE Transactions on Industry Applications, Vol. 46, n. 1, pp. 232-239, Jan/Feb 2010.

[13] Y. Duan, and D.M. Ionel, "A Review of Recent Developments in Electrical Machine Design Optimization Methods With a Permanent-Magnet Synchronous Motor Benchmark Study", IEEE Transactions on Industry Applications, Vol. 49, n. 3, pp. 1268-1275, May/June 2013.

[14] Matsuo, T.; Lipo, T.A., "Rotor design optimization of synchronous reluctance machine," Energy Conversion, IEEE Transactions on , vol.9, no.2, pp.359,365, Jun 1994.

[15] Seok-Hee Han; Jahns, T.M.; Zhu, Z.Q., "Analysis of Rotor Core Eddy-Current Losses in Interior Permanent-Magnet Synchronous Machines," Industry Applications, IEEE Transactions on , vol.46, no.1, pp.196,205, Jan.-feb. 2010

[16] Seok-Hee Han; Jahns, T.M.; Zhu, Z.Q., "Design Tradeoffs Between Stator Core Loss and Torque Ripple in IPM Machines," Industry Applications, IEEE Transactions on , vol.46, no.1, pp.187,195, Jan.-feb. 2010

[17] Staton, D.A.; Miller, T.J.E.; Wood, S.E., "Maximising the saliency ratio of the synchronous reluctance motor," Electric Power Applications, IEE Proceedings B , vol.140, no.4, pp.249,259, Jul 1993.

[18] David H. Wolpert and William G. Macready "No Free Lunch Theorems for Optimization", IEEE TRANSACTIONS ON EVOLUTIONARY COMPUTATION, VOL. 1, NO. 1, APRIL 1997.

[19] D. E. Goldberg, Genetic Algorithms in search, optimization, and Machine Learning. Reading, MA; Addison-Wesley, 1989.

[20] P.J. van Laarhoven and E.H. Aarts, Simulated Annealing: Theory and Applications. Springer, 1987.

[21] F. Neri and V. Tirronen, "Recent advances in differential evolution: A review and experimental analysis," *Artif. Intell. Rev.*, vol. 33, nos. 1–2, pp. 61–106, 2010.

[22] http://www.mathworks.it/matlabcentral/fileexchange/

[23] Kalyanmoy Deb, Amrit Pratap, Sameer Agarwal, and T. Meyarivan, "A Fast and Elitist Multiobjective Genetic Algorithm: NSGA-II", IEEE TRANSACTIONS ON EVOLUTIONARY COMPUTATION, VOL. 6, NO. 2, pp. 182-197, Apr. 2002.

[24] Janez Brest, Saso Greiner, Borko Boskovic, Marjan Mernik, and Viljem Zumer, "Self-Adapting Control Parameters in Differential Evolution: A Comparative Study on Numerical Benchmark Problems", IEEE TRANSACTIONS ON EVOLUTIONARY COMPUTATION, VOL. 10, NO. 6, Dec. 2006, pp. 646-657.

[25] David Meeker, "Finite Element Method Magnetics", Ver. 4.2 User's Manual, February 5, 2009, [Online] available: http://www.femm.info/Archives/doc/manual.pdf

[26] Pellegrino, G.; Guglielmi, P.; Vagati, A.; Villata, F., "Core Losses and Torque Ripple in IPM Machines: Dedicated Modeling and Design Tradeoff," Industry Applications, IEEE Transactions on , vol.46, no.6, pp.2381,2391, Nov.-Dec. 2010

[27] Infolytica MagNet: Design and analysis software for electromagnetics, [Online] available: www.infolytica.com

Francesco Cupertino (M'08, SM'12), received the Laurea degree and the PhD degree in Electrical Engineering from the Politecnico di Bari, Italy, in 1997 and 2001 respectively. From 1999 to 2000 he was with PEMC research group, University of Nottingham, UK. Since July 2002 he is an Assistant Professor at the Politecnico di Bari. His research interests include the design of permanent magnet electrical machines, intelligent motion control of electrical machines, and applications of computational intelligence to control and design. He is the author or co-author of more than 90 scientific papers on these topics. He is the scientific director of the laboratory Energy Factory Bari (EFB), a joint initiative of the Politecnico di Bari and GE AVIO, aimed at developing research projects in the fields of aerospace and energy.

Gianmario Pellegrino (M'06, SM'13), received the M.Sc. and Ph.D. degrees in electrical engineering from Politecnico di Torino, Turin, Italy, in 1998 and 2002, respectively. Since 2002 he is with Politecnico di Torino. His research interests include the design of electrical machines and the control of electrical drives. He is involved in research projects with industry and has more than 20 journal papers and one patent. Dr. Pellegrino is an Associate Editor for the IEEE Transactions on Industry Applications and an IEEE Senior Member. He is the co-recipient of three Prize Paper Awards. He was a guest researcher at Aalborg University, Denmark, in 2002, a visiting fellow at Nottingham University, UK, in 2010/2011, and an honorary fellow at the University of Wisconsin-Madison, USA, in 2013.

Prof. Chris Gerada (M'05) obtained his PhD in Numerical Modelling of Electrical Machines from the University of Nottingham, UK in 2005. He subsequently worked as a researcher at the University of Nottingham on high performance electrical drives and on the design and modelling of electromagnetic actuators for aerospace applications. He was appointed as Lecturer in Electrical Machines in 2008, an Associate Professor in 2011 and Professor in 2013. His core research interests include the design and modelling of high performance electric drives and machines. Prof. Gerada has been the project manager of the GE Aviation Strategic Partnership since 2006 and in 2011 was awarded a Royal Academy of Engineering Senior Research Fellowship supported by Cummins. He is also an Associate Editor for the Transactions in Industry Applications and executive member of the management board of the UK Magnetic Society and the IET Aerospace Technical and Professional Network.